Deciphering the Rules Underlying Xenogeneic Silencing and Counter-Silencing of Lsr2-like Proteins Using CgpS of *Corynebacterium glutamicum* as a Model

Johanna Wiechert,[a] Andrei Filipchyk,[a] Max Hünnefeld,[a] Cornelia Gätgens,[a] Jannis Brehm,[b] Ralf Heermann,[b] [ID] Julia Frunzke[a]

[a]Institut für Bio- und Geowissenschaften, IBG-1: Biotechnologie, Forschungszentrum Jülich, Jülich, Germany
[b]Institut für Molekulare Physiologie, Mikrobiologie und Weinforschung, Johannes-Gutenberg-Universität Mainz, Mainz, Germany

ABSTRACT Lsr2-like nucleoid-associated proteins play an important role as xenogeneic silencers (XS) of horizontally acquired genomic regions in actinobacteria. In this study, we systematically analyzed the *in vivo* constraints underlying silencing and counter-silencing of the Lsr2-like protein CgpS in *Corynebacterium glutamicum*. Genome-wide analysis revealed binding of CgpS to regions featuring a distinct drop in GC profile close to the transcription start site (TSS) but also identified an overrepresented motif with multiple A/T steps at the nucleation site of the nucleoprotein complex. Binding of specific transcription factors (TFs) may oppose XS activity, leading to counter-silencing. Following a synthetic counter-silencing approach, target gene activation was realized by inserting operator sites of an effector-responsive TF within various CgpS target promoters, resulting in increased promoter activity upon TF binding. Analysis of reporter constructs revealed maximal counter-silencing when the TF operator site was inserted at the position of maximal CgpS coverage. This principle was implemented in a synthetic toggle switch, which features a robust and reversible response to effector availability, highlighting the potential for biotechnological applications. Together, our results provide comprehensive insights into how Lsr2 silencing and counter-silencing shape evolutionary network expansion in this medically and biotechnologically relevant bacterial phylum.

IMPORTANCE In actinobacteria, Lsr2-like nucleoid-associated proteins function as xenogeneic silencers (XS) of horizontally acquired genomic regions, including viral elements, virulence gene clusters in *Mycobacterium tuberculosis*, and genes involved in cryptic specialized metabolism in *Streptomyces* species. Consequently, a detailed mechanistic understanding of Lsr2 binding *in vivo* is relevant as a potential drug target and for the identification of novel bioactive compounds. Here, we followed an *in vivo* approach to investigate the rules underlying xenogeneic silencing and counter-silencing of the Lsr2-like XS CgpS from *Corynebacterium glutamicum*. Our results demonstrated that CgpS distinguishes between self and foreign by recognizing a distinct drop in GC profile in combination with a short, sequence-specific motif at the nucleation site. Following a synthetic counter-silencer approach, we studied the potential and constraints of transcription factors to counteract CgpS silencing, thereby facilitating the integration of new genetic traits into host regulatory networks.

KEYWORDS AT-rich DNA, Lsr2, actinobacteria, counter-silencing, horizontal gene transfer, regulatory networks, xenogeneic silencing

Horizontal gene transfer (HGT) is a major driver of bacterial evolution and plays an important role in creating genetic diversity (1). The rapid acquisition of beneficial new traits can create a competitive advantage for the recipient cells (1, 2). However, the chance that foreign DNA decreases the fitness of the cell is high, since it may lead to

interference with regulatory networks, high transcriptional and translational costs, sequestration of cellular machineries, and cytotoxic gene products (3–8). Therefore, bacteria evolved a variety of immune systems allowing them to deal with foreign DNA (9). CRISPR-Cas and restriction modification systems are nuclease-based defense mechanisms enabling the recognition and targeted degradation of invading DNA (10–12). In contrast to these destructive immune systems, xenogeneic silencing enables the tolerance of foreign DNA and consequently fosters the acquisition of novel genetic material into the host chromosome (13). Xenogeneic silencing is based on specific nucleoid-associated proteins (NAPs), so-called xenogeneic silencers (XS) (3). Known XS proteins belong to one of four currently described classes: H-NS-like proteins of proteobacteria, like *Escherichia coli*, *Yersinia*, and *Salmonella* (14–16), MvaT/U-like proteins found in gammaproteobacteria of the *Pseudomonodales* order (17), Lsr2-like XS of *Actinomycetes* (18, 19), and Rok, present in different bacilli, including *Bacillus subtilis* (20, 21). Although XS were convergently evolved and show only low sequence similarity within the different classes, the domain properties of their N-terminal oligomerization domains and their C-terminal DNA-binding domains are similar (19, 20, 22, 23). Their binding mechanisms are diverse, but they all preferentially bind to horizontally acquired DNA, which typically has a higher AT content than the genome of the recipient cell (4, 24). The broad distribution of XS among prokaryotes emphasizes the strong need to discriminate between self and non-self across phylogenetic clades (13). Even so, the GC content of microbial genomes dramatically varies, from 75% (*Actinobacteria*) to less than 20% (bacterial endosymbionts) (25, 26), and horizontally acquired regions typically feature a lower GC content than their resident genome, emphasizing base composition as a major discrimination factor shaping microbial genome evolution (3).

Several studies based on variants defective in oligomer formation revealed that binding of XS proteins to the DNA alone is insufficient for silencing (27–29). The formation of higher-order nucleoprotein complexes instead mediates silencing of the target genes by occlusion or trapping of the RNA polymerase, by interference with the transcription elongation complex, or by enhancing termination (30, 31). To get access to potentially encoded beneficial traits, cells must integrate foreign genes into preexisting regulatory circuits, allowing their controlled expression at appropriate time points and physiological or environmental conditions (32, 33). In contrast to classical activation, counter-silencing is based on the interference of a DNA-binding protein, e.g., a transcription factor (TF), with the silencer-DNA complex leading to transcription initiation without depending on the direct interaction with the RNA polymerase (32, 33). Counter-silencing of H-NS was addressed by several studies either by following a synthetic approach at well-studied promoters (34, 35) or by the analysis of the promoter architectures in the PhoPQ regulatory network (33). The recent study by Will et al. emphasizes that the principle of H-NS xenogeneic silencing and counter-silencing provides a certain degree of flexibility, fostering evolutionary network expansion (33).

Compared to H-NS in proteobacteria, much less is known about Lsr2-like XS proteins conserved throughout the actinobacteria. In *Mycobacterium tuberculosis*, Lsr2 acts as a master regulator of multiple virulence-associated genes (19, 22) and was suggested to be involved in the manifestation of multidrug tolerance (36). The essentiality of Lsr2 for this human pathogen makes this XS protein a highly promising drug candidate (37). In *Corynebacterium glutamicum*, the Lsr2-like XS protein CgpS also was shown to play an essential role as a silencer of cryptic prophage elements whose entrance into the lytic cycle would otherwise cause cell death (4, 38). In contrast to mycobacteria and corynebacterial species, *Streptomyces* species typically encode two Lsr2-like proteins. Here, the prototypical *lsr2* gene, showing the highest sequence identity to mycobacterial Lsr2, was recently described to silence the expression of specialized metabolic clusters (39). Considering the important role of Lsr2 proteins in the medically and biotechnologically important phylum of *Actinobacteria*, a detailed mechanistic understanding of Lsr2 binding *in vivo* is relevant as a potential drug target and for the identification novel bioactive compounds.

In this study, we set out to systematically assess the rules underlying silencing and

counter-silencing of Lsr2-like XS by using the Lsr2-like protein CgpS of *Corynebacterium glutamicum* as a model (4). To the best of our knowledge, this is the first detailed analysis of the counter-silencing mechanism of an Lsr2-like XS protein. Bioinformatic analysis of CgpS ChAP-seq (chromatin affinity purification and sequencing) data revealed a clear preference of CgpS toward AT-rich stretches containing A/T steps (alternation of A to T and vice versa). *In vivo* reporter studies with synthetic promoter variants verified the importance of a distinct drop in GC profile and revealed the overrepresentation of a short, sequence-specific motif at CgpS target regions. Insertion of TF operator sites at different positions within various CgpS target promoters was shown to counteract CgpS silencing, showing the most prominent effect at the position of maximal CgpS binding. With this approach, we provide important insights into the *in vivo* constraints of Lsr2 counter-silencing and contribute to an understanding of how bacteria can evolve control over the expression of horizontally acquired genes.

RESULTS

***In vivo* analysis of CgpS binding preferences.** Recent genome-wide profiling studies revealed that the Lsr2-like xenogeneic silencer CgpS preferentially binds to AT-rich DNA sequences in the genome of *C. glutamicum* ATCC 13032 (4). To determine the parameters affecting CgpS binding and silencing *in vivo*, we systematically analyzed the peak sequences obtained from CgpS ChAP-seq analysis (4) and subsequently verified our conclusion by testing the silencing of synthetic promoter variants. Remarkably, an overlay of the GC profiles of all 35 CgpS target promoters located within the prophage element CGP3 revealed a high degree of similarity with a distinct drop in GC content matching the position of maximal CgpS coverage (Fig. 1A). Genome-wide analysis of AT-rich genomic regions revealed that the fraction of CgpS-bound sequences increased with the length of the particular AT stretch. While increasing numbers of G/C interruptions (occurrence of G or C within an AT stretch) negatively influenced the proportion of CgpS-bound targets (Fig. 1B), a larger number of A/T steps (alternation of A to T and vice versa) increased the fraction of CgpS-bound sequences by trend (Fig. 1C). This trend became especially evident in the case of AT-rich stretches of medium length (14 to 30 bp).

Overall, this analysis suggested that long and consecutive AT stretches represent the main determinant of CgpS target binding. Individual inspection of CgpS-targeted phage promoters revealed a significant correlation between the CgpS peak maximum and the GC minimum in this area (Fig. 1D). Depending on the widths of the CgpS coverage peaks, promoters were grouped into two classes. Class 1 consists of promoters with peak widths between 500 and 850 bp, which typically show one distinct drop in GC profile, while CgpS coverage peaks of class 2 promoters are wider than 850 bp and the corresponding GC profiles often feature broader or multiple drops.

Due to efficient CgpS-mediated silencing of gene expression, most transcriptional start sites (TSS) of CgpS target promoters had not been identified in previous studies (40). It represents, however, an advantage of the chosen model system that expression of the majority of CgpS targets can be induced by triggering prophage induction using the DNA-damaging antibiotic mitomycin C. To provide comprehensive insights into the promoter architecture of CgpS targets, TSS were determined under conditions triggering phage gene expression (600 nM mitomycin C). For 46 out of all 54 CgpS target promoters, at least one TSS was identified (for 31 out of 35 prophage promoters) (see Table S1 in the supplemental material). Strikingly, the analysis of the relative distances between the positions of TSS and maximal CgpS binding revealed that in the majority of CgpS target promoters, TSS are located close to the position of maximal CgpS coverage and GC minimum (Fig. 1D and E; see Table S1 for the complete data set).

Design, build, and test: relevance of a DNA motif for CgpS binding and silencing. Bioinformatic analysis of CgpS target sequences confirmed the preference of CgpS for AT-rich DNA sequences. However, neither the distinct drop in GC content nor the occurrence of long and consecutive AT stretches were unique to CgpS targets (Fig. 1), indicating that additional parameters support CgpS to specifically recognize its
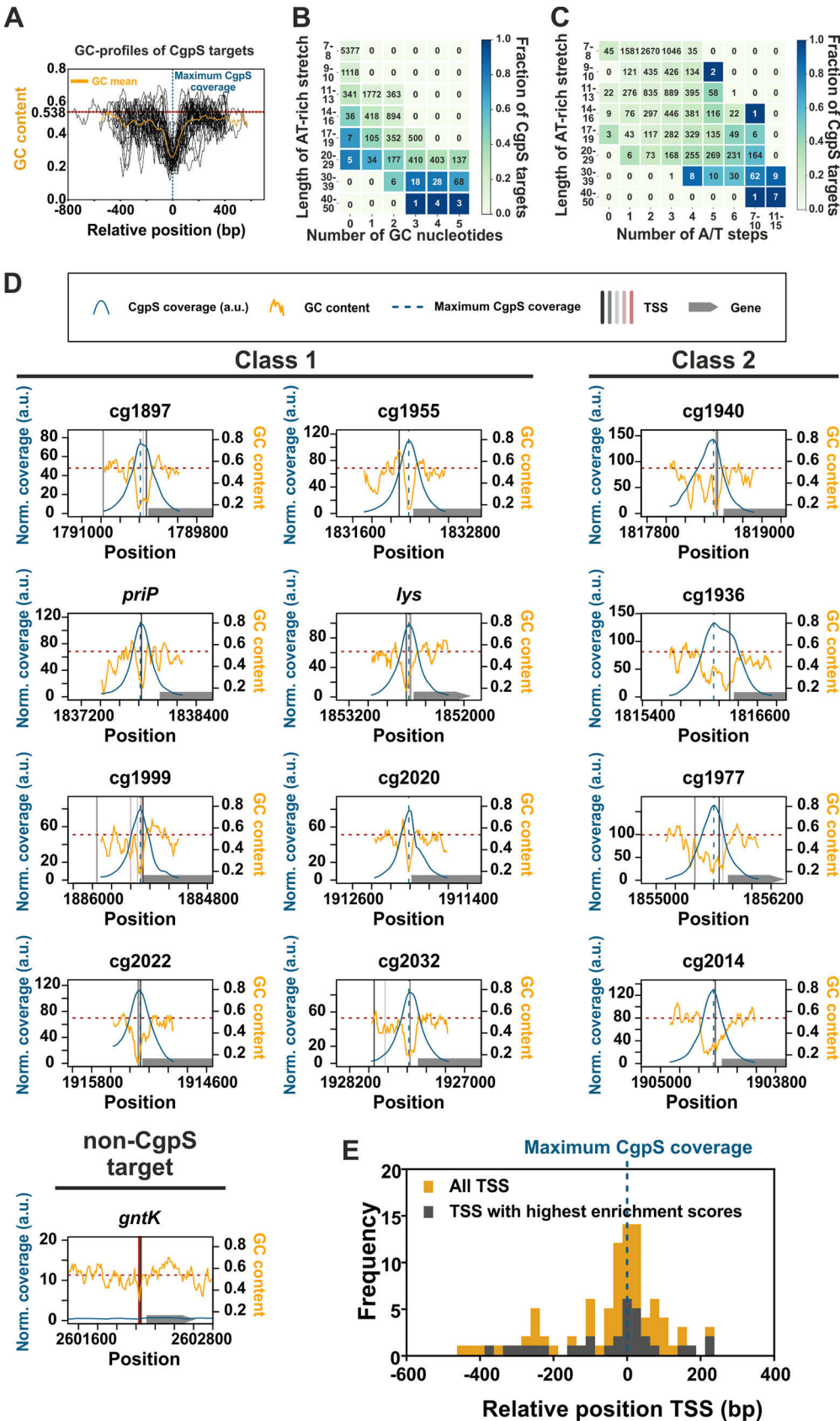
FIG 1 CgpS preferentially binds to long and consecutive AT stretches. (A) Overlay and calculated mean (orange curve) of GC profiles of CgpS target promoters located within the CGP3 prophage (*n* = 35) (4). Profiles were calculated by a

(Continued on next page)

targets. Interestingly, a MEME-ChIP analysis (41) on CgpS-bound promoter sequences revealed a 10-nucleotide-long AT-rich binding motif (E value, 5.2×10^{-9}) containing A/T steps (Fig. 2A), which was found in 51 of 54 bound promoter regions. Remarkably, the presence of this motif within AT-rich stretches of different lengths significantly increased the fraction of CgpS-bound sequences by a factor of up to 2.8-fold (Fig. 2A). However, the genome-wide search for motif occurrence using the online tool FIMO (Find Individual Motif Occurrences) (42) revealed that about 85% of the motifs (669/785) within the *C. glutamicum* genome were not bound by CgpS, indicating that the motif alone is not sufficient to permit CgpS binding.

In the following experiments, we used an *in vivo* approach to test whether the combination of the motif and the drop in GC profile are sufficient for CgpS-mediated silencing of gene expression. For this purpose, different synthetic promoter variants were designed based on the 50- to 70-bp core promoter regions of the phage genes P_{cg1999} and P_{lys}. Both promoters were highly active in the absence of CgpS, indicating that the chosen core regions efficiently drive transcription. In the case of P_{cg1999}, the DNA sequence containing the core promoter elements (-10 and -35 box and TSS) and the predicted binding motif (shown in Fig. 2A) was kept constant (Fig. 2B). The adjacent sequence was either designed to mimic the native GC profile of P_{cg1999} (exchange of A to T and G to C and vice versa, P_{cg1999}_A-T/G-C) or contained a randomized sequence varying in GC profile and sequence (P_{cg1999}_rand). The resulting promoter designs were fused to a gene encoding the yellow fluorescent protein Venus. In line with our hypothesis, the construct P_{cg1999}_A-T/G-C, featuring the native GC profile, was efficiently silenced by CgpS in the wild-type strain and displayed even lower reporter output than the native phage promoter P_{cg1999} (Fig. 2B). Surface plasmon resonance (SPR) analysis revealed CgpS binding kinetics and affinities for this synthetic promoter (equilibrium dissociation constant [K_D], 42 nM) similar to those of the corresponding native CgpS target promoter P_{cg1999} ($K_D = 58$ nM). CgpS also interacted with the control promoter fragment P_{cg3336} but with much lower affinity ($K_D = 381$ nM) and very fast dissociation rates (Fig. 2C). In the prophage-free strain Δphage, which lacks the phage-encoded *cgpS* gene, the reporter output was significantly higher for all tested promoter fusions, confirming that all designs functionally drive transcription. Silencing of the promoter variant with randomized adjacent flanks was strongly impaired, demonstrating that the motif-containing 50-bp core promoter region alone did not mediate silencing. This highlights the importance of the overall drop in GC content observed at CgpS target promoters (Fig. 2B).

The relevance of the identified motif was verified using synthetic promoter designs of the phage promoter P_{lys}. Here, constructs carrying only parts of the predicted motif (70-bp core) did not permit silencing, while constructs covering the motif entirely enabled silencing (Fig. 2D). In all P_{lys}-based synthetic constructs, the native GC profile

FIG 1 Legend (Continued)
rolling mean with a window size of 50 bp and a step size of 10 bp. The GC profiles of the promoters were normalized regarding the orientation and position of the maximal CgpS binding peak (blue line), which was defined for all sequences as position 0. The mean GC content of the *C. glutamicum* genome (69) is shown as a red line (53.8%). (B and C) Genome-wide analysis of CgpS binding to consecutive AT stretches of different lengths considering G/C interruptions (occurrence of G or C within an AT stretch) (B) or number of A/T steps (allowing up to five G/C interruptions) (C). A/T steps are defined as alterations of A to T and vice versa. The value in the array represents the number of stretches found in the *C. glutamicum* genome fitting the respective criteria, while the color indicates the fraction of CgpS targets per array. (D) Inverse correlation of GC profiles and CgpS coverage of CgpS target promoters. CgpS coverage obtained from previous ChAP-seq experiments (4) was calculated with a rolling mean with a window size of 50 and a step size of 10. All identified TSS (see Materials and Methods and Text S1) are shown in Table S1 and represented as vertical black, gray, and red lines (mapped according to their enrichment scores: black > shades of gray > red). Positions of maximal CgpS coverage and average GC content are shown as described for panel A. The corresponding genes are shown as gray arrows. Promoters were grouped into two classes based on the width of the region bound by CgpS (class 1 promoters, 500 to 850 bp, typically featuring one distinct drop in GC profile; class 2 promoters, >850 bp, often broader and containing multiple drops in GC content). As a negative control, the non-CgpS target promoter of the gene *gntK* is shown. a.u., arbitrary units. (E) Frequency distribution of relative positions of all new identified TSS (yellow) of CgpS target promoters referred to the position of maximal CgpS binding. TSS showing the highest enrichment scores per gene are highlighted in gray.
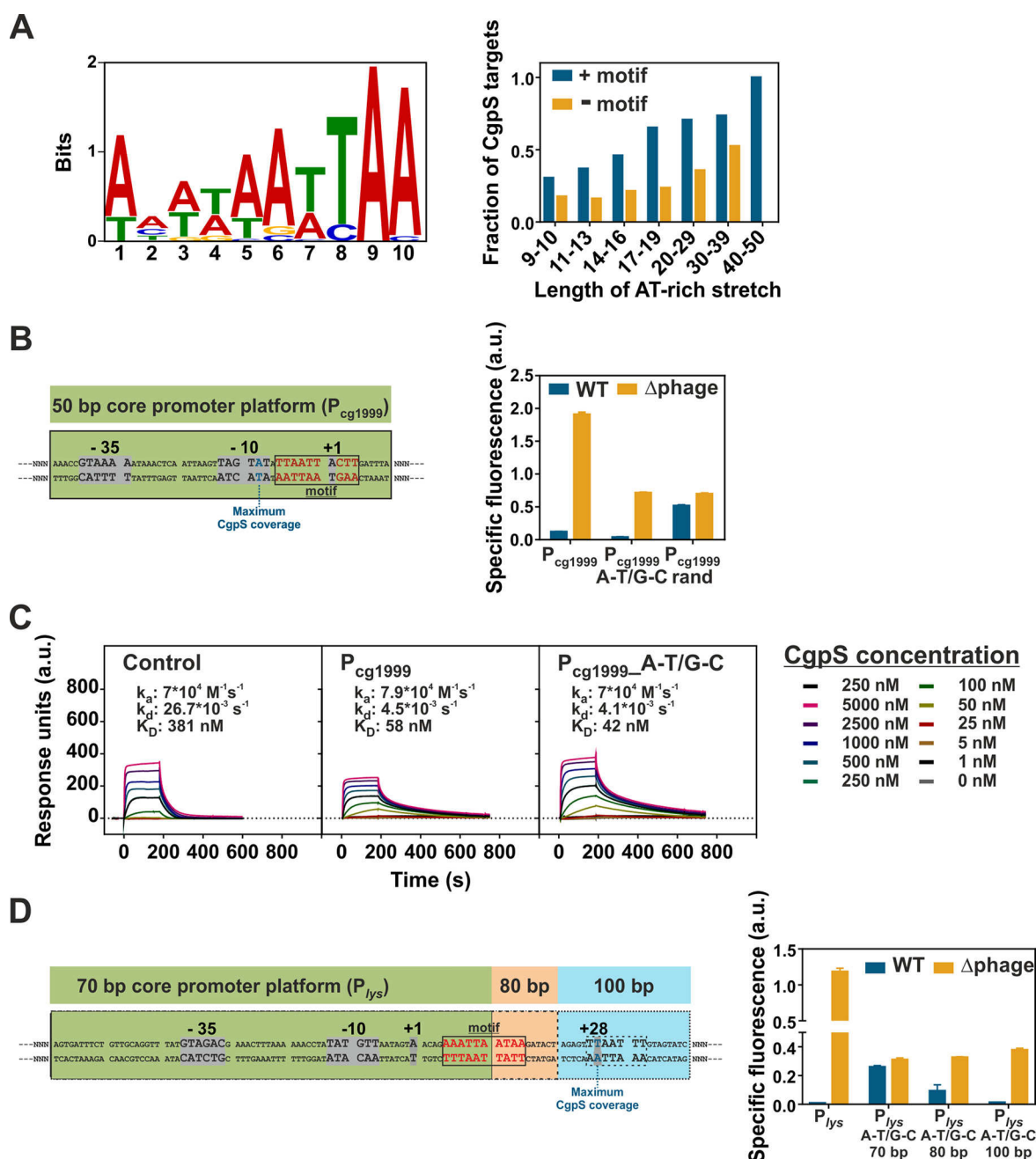
FIG 2 Synthetic *in vivo* approach to dissect the relevance of the GC profile and a sequence-specific binding motif for CgpS silencing. (A) Identified 10-bp CgpS binding motif using MEME-ChIP (41) analysis found within 51 of 54 CgpS target promoters (4) (E value, 5.2×10^{-9}). The bar plot represents the genome-wide fraction of CgpS targets in AT stretches of different length, allowing up to 5 G/C interruptions with or without the identified motif. (B) CgpS silencing of synthetic constructs (P_{cg1999}_A-T/G-C and P_{cg1999}_rand), based on a 50-bp core promoter region (green box) of the phage gene cg1999. The fixed 50-bp DNA sequence covered the -10 and -35 box, positions of the TSS (40), and potential binding motif (gray box). The adjacent sequence (N upstream, 260 bp; N downstream, 48 bp) was either adjusted to maintain the native density of AT stretches (P_{cg1999}_A-T/G-C, exchange of A to T and G to C) or randomized (P_{cg1999}_rand). (C) Surface plasmon resonance analysis of CgpS binding to the synthetic promoter P_{cg1999}_A-T/G-C (423 bp) compared to that of the negative-control P_{cg3336} (424 bp) and the corresponding native CgpS target P_{cg1999} (423 bp). k_a, association constant; k_d, dissociation constant. (D) CgpS silencing of synthetic constructs based on fixed 70- to 100-bp promoter regions of the phage gene *lys*. The 70-bp sequence (green box) covered the -10 and -35 box and TSS but only half of the putative motif. The 80-bp region (green and orange boxes) covered the motif completely, and the 100-bp region (all boxes) additionally covered the position of maximal CgpS coverage. The adjacent sequences (N upstream, 304 bp; N downstream, 70 to 100 bp) were adjusted to maintain the native density of AT stretches (A-T/G-C). (B and D) Reporter outputs (Venus) of the native and corresponding synthetic variants (plasmid backbone pJC1) in wild-type and Δphage (Δ*cgpS*) strains after 5 h of cultivation in a microtiter cultivation system in CGXII medium containing 100 mM glucose. Shown are mean values and standard deviations from biological triplicates. All synthetic sequences are listed in Table S2l.
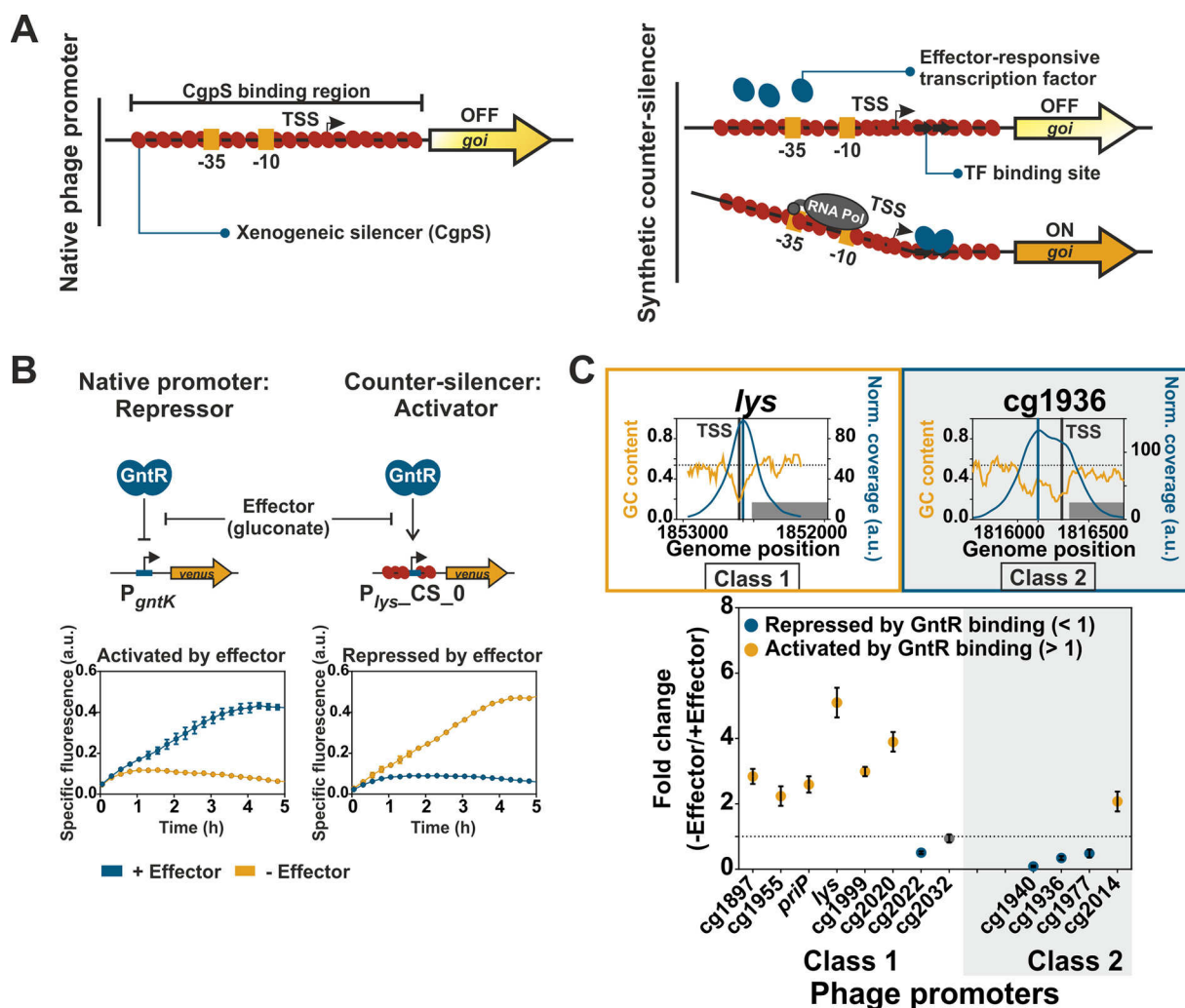
FIG 3 Synthetic approach to study disruptive counter-silencing. (A) Schematic overview of a native CgpS target promoter (phage) and the corresponding synthetic counter-silencer construct. (B) Signal inversion by synthetic counter-silencing. Comparison of the reporter outputs of P$_{gntK}$, the native target promoter of the regulator of gluconate catabolism GntR (43), and the synthetic GntR-dependent counter-silencer promoter P$_{lys}$_CS_0. *C. glutamicum* wild-type strains harboring the plasmid-based constructs (pJC1) were cultivated in the absence of the effector (111 mM glucose) or in its presence (100 mM gluconate) in a microtiter cultivation system. Graphs represent the means and error bars the standard deviations from biological triplicates. Backscatter and fluorescence were measured at 15-min intervals. (C) Counter-silencing efficiency of different phage promoters with inserted GntR binding sites located directly upstream of the position of maximal CgpS binding. Promoters were grouped into two classes based on the width of the region bound by CgpS (class 1 promoters, 500 to 850 bp, often one distinct drop in GC profile; class 2 promoters, >850 bp, often broader or multiple drops in GC content). CgpS coverage and GC profiles of two representative promoters are shown. The highest-ranked TSS are marked as vertical gray lines and the position of maximal CgpS binding as vertical blue lines. GC profiles of all used phage promoters are shown in Fig. 1D. *C. glutamicum* wild-type cells harboring the plasmid-based (pJC1) counter-silencers were cultivated in the presence (100 mM gluconate) or absence (100 mM glucose) of the effector molecule gluconate in a microtiter cultivation system. Fold change ratios of Venus reporter outputs in the absence and in the presence of the effector were calculated based on the specific reporter outputs after 5 h of cultivation (Fig. S1A). Dots represent the means and error bars the standard deviations from at least biological triplicates. Yellow dots demonstrate counter-silencing (activated by GntR binding), while blue dots represent repression (repressed by GntR binding). Promoters, which did not show significant changes in reporter output, are shown as gray dots (*t* test; *P* < 0.05).

of the sequence flanking the core promoter region was mimicked but the DNA sequence was changed (A to T and G to C and vice versa). This *in vivo* analysis of synthetic phage promoter variants revealed that efficient CgpS silencing depended on both specific DNA sequences (binding motif) and the drop in GC profile.

Synthetic disruptive counter-silencing. Disruptive counter-silencing was previously described as a mechanism that may provide access to horizontally acquired genes silenced by nucleoid-associated proteins (32). To study the potential and constraints of evolutionary network expansion by counter-silencing of CgpS target promoters, a synthetic counter-silencer (CS) design was applied in this study (Fig. 3A). At native

target promoters (e.g., P_{cg1999} or P_{lys}), oligomerization of the xenogeneic silencer CgpS leads to the formation of a nucleoprotein complex inhibiting transcription (4, 31). In the following experiments, we used a set of 12 different phage promoters as a basis for synthetic CS constructs and inserted the operator sequence of an effector-responsive transcription factor (TF) into the silenced promoter regions. We postulated that binding of the TF to its operator sequence would interfere with the silencer nucleoprotein complex and thereby mediate counter-silencing (Fig. 3A). To avoid interference of the inserted operator site with CgpS-mediated silencing, we chose the operator site of the functionally redundant TFs GntR1 (Cg2783) and GntR2 (Cg1935) (summarized as GntR in the following), which bind to a well-defined short (15 bp) and AT-rich (GC content, 27%) DNA motif (43). One of the native targets of GntR is the promoter of the *gntK* gene, which is repressed by binding of GntR. The P_{gntK} promoter and the synthetic promoter constructs were fused via a consistent linker containing a ribosomal binding site (RBS) to the reporter gene *venus* and were inserted into the plasmid pJC1. The effector molecule gluconate was shown to act as an inducer triggering the dissociation of GntR from its operator site (43), consequently leading to derepression of P_{gntK} (Fig. 3B).

Monitoring of fluorescent outputs driven by phage-based synthetic promoter constructs allows the *in vivo* analysis of silencing and counter-silencing efficiencies. GntR operator sites were indeed confirmed as suitable candidates for the construction of counter-silencers, since the insertion into different phage promoters led to only slightly increased background expression levels in the wild-type strain in the presence of the effector molecule (Fig. S1A). The insertion of a GntR binding site (BS) within the CgpS-silenced phage promoter P_{lys} ($P_{lys}\_CS\_0$) led to effector-dependent reporter outputs. GntR binding resulted in an increased reporter output of the counter-silencer construct $P_{lys}\_CS\_0$ when glucose was added as a carbon source, while gluconate (effector addition) triggered the dissociation of GntR, leading to silencing of promoter activity by CgpS (Fig. 3B). This is especially remarkable considering that the binding site was inserted at the position of maximal CgpS coverage close to the annotated TSS (27 bp downstream [Table S1]). Based on textbook knowledge, this position would rather fit to a repressor function (44, 45). In the case of P_{gntK}, the GntR binding site overlaps the TSS, leading to repression of gene expression (43). In the context of xenogeneic silencing, however, GntR binding appeared to efficiently interfere with CgpS silencing. Thus, in contrast to the native GntR target P_{gntK}, the synthetic P_{lys}-counter-silencer promoter was activated in the absence of the effector molecule. Although both promoters (P_{gntK} and $P_{lys}\_CS\_0$) were completely different and had only the 15-bp-long GntR binding site in common, they showed very similar but inverted responses to effector availability (Fig. 3B). This demonstrates the potential of the counter-silencing principle to convert a repressor to an activating, tunable counter-silencer, thereby facilitating the expansion of regulatory networks.

Disruptive counter-silencing is most efficient at the CgpS nucleation site. To systematically assess the constraints of counter-silencing, 12 representative phage promoters of both classes (eight class 1 and four class 2) were selected as targets to test the efficiency of synthetic counter-silencing. The GntR binding site was inserted directly upstream of the previously identified position of maximal CgpS binding obtained from ChAP-seq analysis (4). To study counter-silencing efficiency, all constructs were analyzed in *C. glutamicum* wild-type cells in the presence and absence of the effector molecule gluconate. The ratio of maximal (− effector; GntR binding) and minimal (+ effector; GntR dissociation) reporter outputs was used to compare the counter-silencing efficiency of the different constructs (Fig. 3C and Fig. S1). Overall, counter-silencing appeared to be more efficient in class 1 promoters typically featuring a bell-shaped CgpS peak and a distinct drop in GC profile. Here, six out of eight constructs showed an effector-responsive counter-silencing behavior. In contrast, only one of four class 2 promoters was activated by GntR binding. The broader regions bound by CgpS are probably stabilizing the silencer-DNA complex, compensating for the local interference
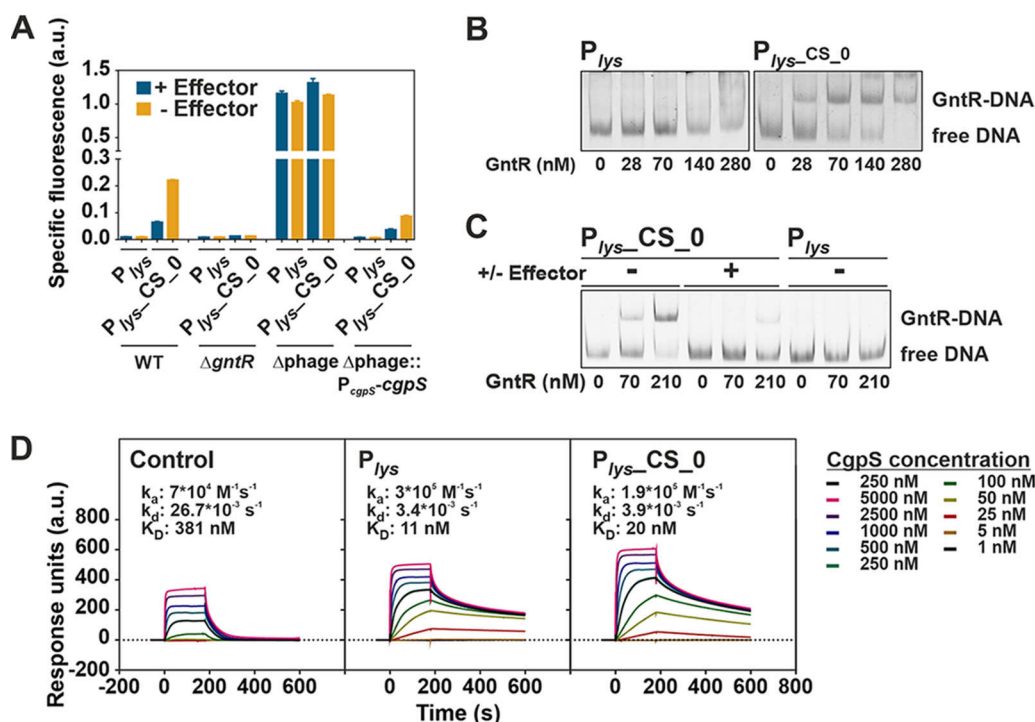
FIG 4 Silencing is mediated by CgpS, while counter-silencing depends of GntR binding. (A) Reporter output (*venus* expression) of different *C. glutamicum* strains carrying the native P*lys* promoter or the counter-silencing design P*lys*_CS_0 after 5 h of cultivation. Both constructs were analyzed in *C. glutamicum* wild-type cells, in a *gntR1-gntR2* double deletion strain, in the prophage-free strain Δphage (lacking the phage-encoded *cgpS*), and in its variant with reintegrated *cgpS* under the control of its native promoter (Δphage::P*cgpS*-*cgpS*). Cells were cultivated in a microtiter cultivation system in CGXII medium supplemented with either 100 mM gluconate (+ effector) or 100 mM fructose (− effector). (B) EMSA of GntR binding to DNA fragments covering the synthetic counter-silencer promoter P*lys*_CS_0 (533 bp, 14 nM) or the native phage promoter P*lys* (518 bp, 14 nM). (C) Impact of the effector molecule gluconate on binding of GntR to the synthetic counter-silencer construct. EMSA was performed as described for panel B, but GntR and the DNA fragments were incubated either in the presence of the effector (100 mM gluconate) or in its absence (100 mM glucose). (D) Surface plasmon resonance analysis of CgpS binding kinetics to biotinylated DNA fragments covering the negative-control P*cg3336* (424 bp), the native phage promoter P*lys* (424 bp), or the corresponding synthetic counter-silencer construct (439 bp) that were captured onto a streptavidin-coated sensor chip. Different concentrations of CgpS were passed over the chip using a contact (association) time of 180 s, followed by a 420-s dissociation phase. The increase in response units correlates with increasing CgpS concentrations.

effects caused by GntR binding. The general functionality of promoter variants (Fig. S1A) was confirmed in the strain Δphage, where all variants showed a significant fluorescent signal (Fig. S1B). Interestingly, GntR binding to P*cg2014* led to counter-silencing in the wild type but to slight repression in the Δphage strain, suggesting that only the destructive interference between CgpS and GntR facilitates efficient transcription of the downstream gene.

Silencing is mediated by CgpS binding, and counter-silencing depends on GntR binding. CgpS as silencer and GntR as counter-silencer are the two key components of the synthetic counter-silencer approach presented in this study. To confirm their presumed functions, mutant analysis and *in vitro* binding assays with both proteins were performed. The reporter outputs of the native phage promoter P*lys* as well as of the corresponding counter-silencer construct (P*lys*_CS_0) were analyzed in *C. glutamicum* wild-type cells and different mutant strains. In the wild type, the counter-silencing construct showed the expected increase of reporter output upon GntR binding (− effector). In line with the assumed counter-silencing function of GntR, both constructs featured a low reporter output in the Δ*gntR* strain lacking both functionally redundant GntR1 and GntR2 regulators (Fig. 4A). To confirm the relevance of the inserted GntR operator sequence, different mutated variants were tested as well. Here, neither the insertion of a randomized operator sequence, identical in length and nucleotide

composition, nor a mutated operator site, where only one conserved base in the GntR motif was exchanged, led to counter-silencing of the P_{lys} promoter (Fig. S2). These results confirmed that counter-silencing directly depends on GntR binding. However, the insertion of a reverse-oriented GntR binding site within the silenced promoter allowed counter-silencing, showing that this mechanism does not depend on the directionality of the binding site (Fig. S3). P_{lys} and the corresponding counter-silencer construct showed strongly increased promoter activities in the Δphage strain in the absence of CgpS, suggesting that CgpS is responsible for silencing. Effector-dependent activation was abolished in the absence of CgpS, indicating that GntR acts as a counter-silencer rather than as a classical activator. Reintegration of the *cgpS* gene into the Δphage strain, resulting in Δphage::P_{cgpS}-*cgpS*, confirmed CgpS as the only factor responsible for silencing of the native phage promoter P_{lys} and, thus, emphasized that CgpS function does not depend on further phage-encoded accessory proteins (Fig. 4A).

As a further piece of evidence, electrophoretic mobility shift assays (EMSA) were performed to confirm the specific binding of GntR to the synthetic counter-silencing construct (P_{lys}_CS_0) *in vitro*. In contrast to the native phage promoter, the P_{lys} fragment containing the GntR operator site showed a significant shift at low GntR concentrations, confirming specific GntR binding to P_{lys}_CS_0 (Fig. 4B). Addition of the effector molecule gluconate led to dissociation of GntR (Fig. 4C), which is in agreement with previous reports (43). Surface plasmon resonance analysis of CgpS binding to DNA fragments covering either P_{lys} or the synthetic counter-silencer construct P_{lys}_CS_0 showed comparable high-affinity binding of CgpS to both promoters (K_D, P_{lys}, 11 nM; P_{lys}_CS_0, 20 nM) (Fig. 4D).

Impact of operator site position. When analyzing the promoter architecture of horizontally acquired gene clusters, previous studies revealed a certain variability (33). To systematically assess the potential and constraints of the counter-silencing mechanism for evolutionary network expansion, we analyzed the impact of operator site position on counter-silencing efficiency. Therefore, the GntR binding site was inserted at different positions using the prophage promoter P_{lys} as a test case (Fig. 5A). Position 0 is defined as the position located directly upstream of the nucleotide featuring maximal CgpS binding in ChAP-seq studies (4). The position of maximal CgpS binding was located 27 bp downstream of the TSS. *C. glutamicum* wild-type cells harboring the plasmid-based constructs [pJC1-P_{lys}::GntR BS_pos(variable)-*venus*] were cultivated in the presence or absence of the effector molecule gluconate. Induced and noninduced reporter outputs were strongly influenced by the binding site position. This demonstrated that the inserted binding site itself, depending on its position, already interferes with the silencer-DNA complex (Fig. 5B). Comparison of the fold change ratio of reporter outputs in the absence and presence of the effector gluconate revealed that the construct with the GntR binding site located directly upstream of the maximal CgpS binding peak (position 0) showed the highest dynamic range (~5-fold). This dynamic range decreased when the operator was inserted between 15 bp upstream (−15) and 10 bp downstream (+10) of the maximal CgpS binding peak, but constructs still showed counter-silencing in the absence of the effector (Fig. 5C). However, analyzing the −15 promoter variant in the absence of CgpS (Δphage) revealed repression caused by GntR binding, demonstrating again that the observed counter-silencing effect is a result of regulatory interference (Fig. S4). GntR binding sites located at greater distances led in most cases to relatively low reporter outputs. Here, the expression level tended to be higher when GntR binding was inhibited, suggesting GntR acts mainly as a repressor of gene expression at these positions (Fig. 5B and C). A similar trend was observed for the phage promoter P_{cg1999} (Fig. S5). Altogether, these results demonstrated that the impact of GntR binding on promoter activity strongly depends on the context of xenogeneic silencing. While interference with CgpS binding triggered promoter activation by counter-silencing, GntR binding in the absence of CgpS often lowered the reporter output. Analysis of reporter outputs driven by 5′-truncated promoter variants of P_{lys} and P_{lys}_CS_0 revealed that the region >89 bp upstream of
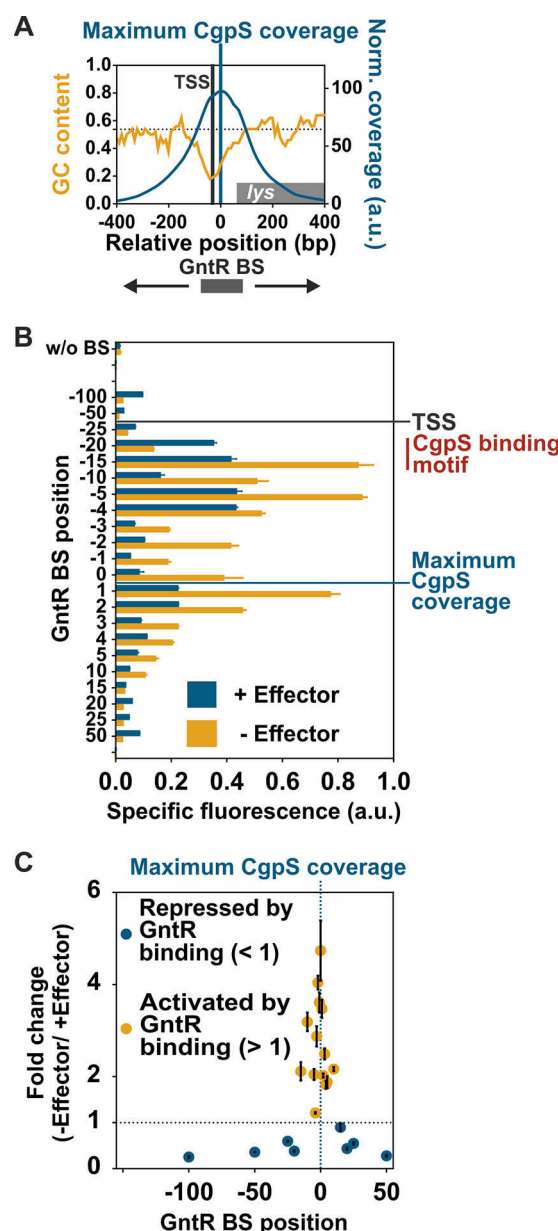
FIG 5 Impact of GntR operator position on inducibility of P$_{lys}$-based promoter constructs. (A) Inverse correlation of GC profile and CgpS binding coverage (4) of the phage promoter P$_{lys}$. The transcriptional start site (TSS) and the position of maximal CgpS binding are shown as vertical lines. Binding site positions (also used in panels B and C) refer to the sequence base associated with maximal CgpS binding. The position directly upstream of this nucleotide was defined as position 0. (B) Impact of inserted GntR binding site position on specific reporter outputs in the presence (gluconate) and absence (glucose) of the effector molecule after 5 h of cultivation. Positions of TSS and maximal CgpS coverage are marked by horizontal lines, and the range of the putative CgpS binding motif is shown. (C) Impact of GntR binding site position on counter-silencing efficiency of P$_{lys}$-based promoter constructs. Ratio of specific reporter outputs, shown in panel B, were used for the calculation of their inducibility (fold change). Cells harboring the plasmid-based synthetic promoter constructs were grown in CGXII medium supplemented with either 111 mM glucose or 100 mM gluconate. Bars (B) and dots (C) represent the means and error bars the standard deviations from at least biological triplicates.

the maximal CgpS binding peak is not required for silencing or counter-silencing (Fig. S6).

Implementation in a genetic toggle switch. The P$_{lys}$ counter-silencing construct (P$_{lys}$_CS_0) and the native GntR target promoter P$_{gntK}$ showed a very similar promoter output but an inverted response to effector availability. While P$_{gntK}$ is repressed by
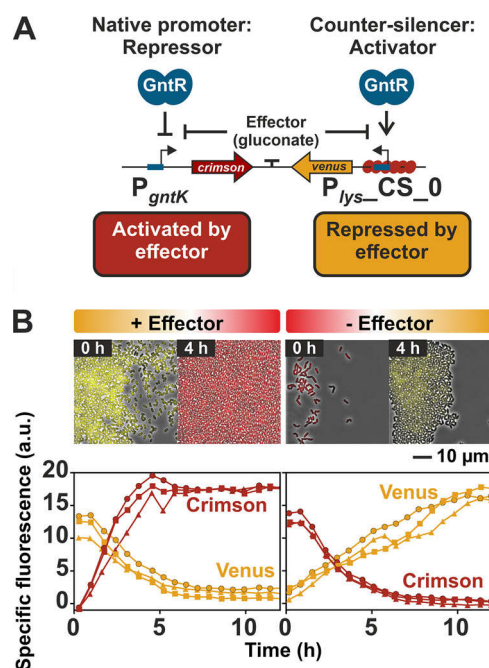
FIG 6 Implementation of P_{gntK} and $P_{lys\_}$CS_0 in a genetic toggle switch. (A) Scheme of the designed toggle switch based on the native GntR target promoter P_{gntK} and the synthetic GntR-dependent P_{lys} counter-silencer construct. In order to monitor their activities, the promoters were fused to different reporter genes ($P_{lys\_}$CS_0-*venus* and P_{gntK}-*e2-crimson*). The promoter reporter gene fusions were oriented in opposite directions and separated by a short terminator sequence. (B) Dynamic switch between both reporter outputs. *C. glutamicum* wild-type cells harboring the plasmid-based toggle were cultivated in a microfluidic cultivation system (46) with continuous supply of CGXII medium supplemented either 111 mM glucose or 100 mM gluconate and analyzed by time-lapse microscopy at 20-min intervals. Switch of carbon source supply was performed after the first 17 h. This time point was defined as T_0. The graphs show the specific fluorescence of three independent microcolonies (circles, squares, and triangles) over time, and images display one representative colony.

binding of GntR, the counter-silencer promoter is activated by GntR binding in the absence of the effector molecule gluconate (Fig. 3B). Both promoters were combined in a gluconate-dependent, GntR-controlled genetic toggle switch. To monitor the switching between different expression states, $P_{lys\_}$CS_0 was fused to the reporter gene *venus*, while the native GntR target promoter P_{gntK} was fused to the reporter gene *e2-crimson* (Fig. 6A). Since the toggle output is only regulated by GntR binding, native GntR levels could be used for toggle control, avoiding a negative impact of artificial TF levels on cellular growth. *C. glutamicum* wild-type cells harboring the plasmid-based toggle (pJC1-$P_{lys\_}$CS_0-*venus*-T-P_{gntK}-*e2-crimson*) were cultivated in a microfluidic chip device (46) in minimal medium containing either gluconate (+ effector) or glucose (− effector) as carbon source. The carbon sources were switched after the first 17 h. The following time-lapse microscopy analysis revealed that the output of this synthetic toggle is reversible, as shown by the rapid changes in reporter outputs (Fig. 6B). This overall design principle allows the control of the toggle by only one specific effector-responsive TF and features a robust and reversible response to effector availability, highlighting the potential of this toggle for biotechnological applications, for example, to switch between biomass production and product formation.

DISCUSSION

The nucleoid-associated protein Lsr2 is conserved throughout the phylum of *Actinobacteria*, where it plays an important role in the xenogeneic silencing of horizontally acquired genomic regions (4, 18, 19, 39). The Lsr2-like protein CgpS was recently described as a classical XS protein silencing the expression of cryptic prophage elements and further horizontally acquired elements in *C. glutamicum* (4).

CgpS binds DNA with a distinct drop in GC content close to the TSS. In this study, we systematically assessed the promoter architecture of CgpS targets as well as the constraints underlying silencing and counter-silencing of target gene expression. The genome-wide analysis of CgpS-bound regions obtained from ChAP-seq analysis revealed that CgpS targets share a distinct drop in GC content (Fig. 1). The binding to AT-rich DNA is a common feature of XS proteins (3) and was shown to represent an important fitness trait to avoid spurious transcription and the sequestering of the RNA polymerase (8). The importance of this drop in GC content was confirmed by measuring the CgpS-mediated silencing of P_{cg1999}-based synthetic variants, where changes in GC profile abolished silencing (Fig. 2B). The analysis of relative distance between the TSS and position of maximal CgpS binding emphasized that binding of CgpS close to the TSS is important for efficient silencing (Fig. 1E).

CgpS recognizes a sequence-specific binding motif containing A/T steps. *In vitro* protein binding microarray experiments revealed a clear preference of the xenogeneic silencers H-NS, MvaT, and Rok for DNA stretches containing flexible TpA (thymine-p-adenine) steps, while no positive effect of TpA steps was observed for Lsr2 from *Mycobacterium tuberculosis* (20, 47). Our design-test-build approach, where different synthetic promoter variants were tested *in vivo* concerning CgpS-mediated silencing, however, revealed a certain degree of sequence specificity of CgpS toward a binding motif containing A/T steps. While the GC content was kept constant, alteration of the proposed motif in the P_{lys} promoter significantly affected *in vivo* silencing (Fig. 2). A scenario that has been proposed for H-NS features a high affinity toward DNA (K_D of 60 nM), allowing the scanning of DNA until it reaches high-affinity sites, triggering the nucleation of the tight nucleoprotein complex required for silencing (3, 48, 49). Based on the systematic analysis of truncated promoter variants, we clearly defined the region required for efficient *in vivo* silencing by CgpS (see Fig. S6 in the supplemental material). It is important to note that we almost exclusively relied on *in vivo* approaches, including ChAP-seq analysis and reporter assays, to define the parameters affecting silencing and counter-silencing at the systems level. Although *in vitro* analysis of protein-DNA fragments (often linear DNA) is frequently applied and has provided valuable insights into the binding behavior of XS proteins (20, 47, 49), the conditions do not reflect physiologically relevant situations (DNA topology, protein-protein inter-action, and interference); consequently, the results have to be interpreted with caution.

GntR-dependent counter-silencing is a disruptive mechanism. While xenogeneic silencing neutralizes the potentially negative effect of invading foreign DNA, counter-silencing allows the integration into the host regulatory network and thereby provides access to horizontally acquired genes. This principle has been almost exclusively studied for H-NS in proteobacteria, and several types of TFs were shown to counteract H-NS silencing *in vivo* (15, 50–53). In the case of Lsr2, the mycobacterial iron-dependent regulator IdeR represents, to the best of our knowledge, the only example of an investigated Lsr2 counter-silencer. IdeR enables the iron-dependent activation of fer-ritin by alleviating Lsr2 repression at the *bfrB* locus (54).

During bacterial evolution, mutations leading to the formation of TF operator sequences within silenced promoters allow the controlled expression of the previously silenced genes by TF-mediated counter-silencing. In this work, the artificial insertion of the 15-bp short operator sequences of the gluconate-dependent TF GntR within different CgpS target promoters allowed us to study the potential and constraints of counter-silencing of this Lsr2-like XS protein. Binding of GntR to several CgpS target promoters led to transcription initiation of the silenced phage promoters, demonstrat-ing that small changes in the DNA sequence added a further regulatory layer for expression control.

All tested CgpS target promoters showed significant reporter output in the absence of CgpS, confirming that they promote transcription and that CgpS inhibits promoter activity, presumably by hindering open complex formation or by trapping the open complex once it has formed (55). Previous studies already suggested that, without

xenogeneic silencing, open complex formation is typically not the rate-limiting step at AT-rich promoters of horizontally acquired genes, meaning they are constitutively active (33, 56, 57). In the case of the H-NS target promoter *pagC*, an *in vitro* approach demonstrated RNA polymerase binding and open complex formation in the absence of additional factors, confirming that this promoter alone is transcriptionally competent (33).

In general, two different mechanisms of counter-silencing are conceivable. In one scenario (disruptive mechanism), the interference of TF and XS protein leads to a local disruption of the XS nucleoprotein complex, thereby enabling binding of the RNA polymerase to the DNA. Another possibility is that counter-silencing allows for supportive contacts between the RNA polymerase and the TF itself or more distal DNA regions (supportive mechanism). In this study, binding of GntR to the promoter constructs in the absence of the XS CgpS resulted in reduced reporter outputs, although counter-silencing was observed in the wild type. This result strongly speaks for a disruptive rather than a supportive GntR-mediated counter-silencing mechanism.

GntR binding close to the CgpS nucleation site is a prerequisite for efficient counter-silencing. By the systematic analysis of promoter variants with varied positions of the GntR operator site, we clearly defined the window where binding of a specific TF led to counter-silencing. Counter-silencing of the Lsr2-like XS CgpS was most efficient at positions close to the position of maximal CgpS binding in a range of approximately 25 bp (Fig. 5 and Fig. S5), demonstrating that the position of GntR binding is critical for counter-silencing.

Previous studies by Will et al. revealed that counter-silencing and classical activation are different mechanisms of gene regulation (33). While TFs acting as activators typically bind to conserved promoter architectures and promote transcription either by changing the DNA conformation or by recruiting the RNA polymerase (58), the principle of counter-silencing allows a higher degree of flexibility in terms of promoter architecture (33). For the PhoPQ regulon of *Salmonella enterica* serovar Typhimurium, it was shown that PhoP activates core promoters featuring a precise operator position overlapping the −35 box. In contrast, horizontally acquired PhoP target genes show rather diverse promoter architectures, and here transcriptional activation is achieved by counter-silencing of H-NS. In these reported examples, the distances between the TSS and the closest PhoP binding site vary by only 34 bp (33, 59). This is in a range similar to that for our results and those obtained in previous studies for the H-NS target promoter P$_{bgl}$, where the insertion of TF operator sites counteracted H-NS silencing in a comparable window (34).

It is intriguing that in the context of xenogeneic silencing binding of a TF at positions close to the TSS leads to promoter activation, where it would cause a block of transcription at classical promoters (44, 60). Indeed, GntR binding in the absence of the XS CgpS resulted in reduced reporter outputs of several synthetic promoter constructs tested in this study (Fig. S1 and S4). However, counter-silencing was observed in the presence of CgpS in the wild type. These results demonstrate the potential of the counter-silencing principle to convert a repressor to an activating, tunable counter-silencer, thereby facilitating the integration of horizontally acquired DNA into host regulatory networks. Overall, these data illustrate how interference of TFs is shaping global regulatory networks and that the regulatory impact of TF binding is strongly affected by competition with other DNA-binding proteins.

MATERIALS AND METHODS

Bacterial strains and cultivation conditions. All bacterial strains and plasmids used in this project are listed in Table S2A to C in the supplemental material. The strain *C. glutamicum* ATCC 13032 (61) was used as the wild-type strain. Detailed information about general growth conditions, microtiter cultivations used to monitor cell growth and fluorescence (62), and cultivations in the microfluidic chip device (46, 63) is available in the supplemental material (Text S1).

Recombinant DNA work. All standard molecular methods, such as PCR, DNA restriction, and Gibson assembly, were performed according to previously described standard protocols (64, 65) or according to the manufacturer's instructions. All plasmids were constructed by Gibson assembly. Details on plasmid construction are provided in Table S2C. DNA sequencing and synthesis of oligonucleotides used for

amplification of DNA fragments (inserts for Gibson assembly [Table S2D], biotinylated DNA fragments for surface plasmon resonance [SPR] spectroscopy [Table S2E], and DNA fragments for electrophoretic mobility shift assays [EMSA] [Table S2F]) and sequencing (Table S2G), as well as synthesis of DNA sequences (Table S2H), were performed by Eurofins Genomics (Ebersberg, Germany). Chromosomal DNA of *C. glutamicum* ATCC 13032 was used as the PCR template and was prepared as described previously (66). Detailed information about construction of strain Δphage::P$_{cgpS}$-*cgpS* via two-step homologous recombination (67) and the design of disruptive counter-silencing constructs is available in the supplemental material (Text S1).

Determination of TSS. The determination of TSS and data analysis were performed with *C. glutamicum* wild-type cells by Vertis Biotechnology AG (Freising, Germany) using the Cappable-seq method developed by Ettwiller and Schildkraut (68). Prophage induction was triggered by adding mitomycin C. Detailed information about cultivation conditions, RNA preparation, and data analysis can be found in the supplemental material (Text S1). Relevant TSS were assigned to phage and nonphage CgpS target promoters when they were located in the promoter region 500 bp upstream of the start codon and directed in gene orientation (Table S1). Multiple TSS assigned to the same promoter were ranked depending on their enrichment scores.

Plots of CgpS coverage and GC profiles. Normalized CgpS coverage values obtained from previous ChAP-seq analysis of Pfeifer and colleagues (4) and GC content of the reference *C. glutamicum* genome BX927147 (69) were plotted to the corresponding genome positions. Both parameters were calculated by a rolling mean with a window size of 50 bp and a step size of 10 bp using R (http://www.R-project.org) (70). The position of maximal CgpS coverage was centered, and the promoter orientation was normalized (start codon of the corresponding gene is located on the right site). Identified TSS positions were added. Ends of graphs are defined by the range of the CgpS binding peaks identified in previous ChAP-seq analysis (4). Plotting was performed either by R (70) or by GraphPad Prism 7.00 (GraphPad Software, La Jolla, CA).

Analyses of AT-rich stretches in CgpS binding regions. The *C. glutamicum* genome (BX927147 [69]) was scanned for AT-rich stretches using a custom python script (submitted to GitHub at https://github.com/afilipch/afp/blob/master/genomic/get_at_stretches.py). For further details, see the supplemental material (Text S1).

Protein purification, SPR spectroscopy, and EMSA. Information about purification of Strep-tagged CgpS and His-tagged GntR and the performed *in vitro* binding assays (SPR spectroscopy and EMSA) can be found in the supplemental material (Text S1).

Data availability. The custom python script used for scanning for AT-rich stretches is available in the GitHub repository (https://github.com/afilipch/afp/blob/master/genomic/get_at_stretches.py). Data from previously reported ChAP-seq analysis (4) are available at the GEO database (https://www.ncbi.nlm.nih.gov/geo) under accession number GSE141132.

SUPPLEMENTAL MATERIAL

Supplemental material is available online only.

TEXT S1, PDF file, 0.2 MB.
FIG S1, TIF file, 0.2 MB.
FIG S2, TIF file, 0.2 MB.
FIG S3, TIF file, 0.1 MB.
FIG S4, TIF file, 0.1 MB.
FIG S5, TIF file, 0.3 MB.
FIG S6, TIF file, 0.2 MB.
TABLE S1, XLSX file, 0.03 MB.
TABLE S2, DOCX file, 0.1 MB.

ACKNOWLEDGMENTS

REFERENCES

1. Ochman H, Lawrence JG, Groisman EA. 2000. Lateral gene transfer and the nature of bacterial innovation. Nature 405:299–304. https://doi.org/10.1038/35012500.

2. Dorman CJ. 2014. H-NS-like nucleoid-associated proteins, mobile genetic elements and horizontal gene transfer in bacteria. Plasmid 75:1–11. https://doi.org/10.1016/j.plasmid.2014.06.004.

3. Navarre WW. 2016. The impact of gene silencing on horizontal gene transfer and bacterial evolution. Adv Microb Physiol 69:157–186. https://doi.org/10.1016/bs.ampbs.2016.07.004.

4. Pfeifer E, Hünnefeld M, Popa O, Polen T, Kohlheyer D, Baumgart M, Frunzke J. 2016. Silencing of cryptic prophages in *Corynebacterium glutamicum*. Nucleic Acids Res 44:10117–10131. https://doi.org/10.1093/nar/gkw692.

5. Vogan AA, Higgs PG. 2011. The advantages and disadvantages of horizontal gene transfer and the emergence of the first species. Biol Direct 6:1. https://doi.org/10.1186/1745-6150-6-1.

6. Park C, Zhang J. 2012. High expression hampers horizontal gene transfer. Genome Biol Evol 4:523–532. https://doi.org/10.1093/gbe/evs030.

7. Baltrus DA. 2013. Exploring the costs of horizontal gene transfer. Trends Ecol Evol 28:489–495. https://doi.org/10.1016/j.tree.2013.04.002.

8. Lamberte LE, Baniulyte G, Singh SS, Stringer AM, Bonocora RP, Stracy M, Kapanidis AN, Wade JT, Grainger DC. 2017. Horizontally acquired AT-rich genes in *Escherichia coli* cause toxicity by sequestering RNA polymerase. Nat Microbiol 2:16249. https://doi.org/10.1038/nmicrobiol.2016.249.

9. Doron S, Melamed S, Ofir G, Leavitt A, Lopatina A, Keren M, Amitai G, Sorek R, Doron S, Melamed S, Ofir G, Leavitt A, Lopatina A, Keren M, Amitai G, Sorek R. 2018. Systematic discovery of antiphage defense systems in the microbial pangenome. Science 359:eaar4120. https://doi.org/10.1126/science.aar4120.

10. Labrie SJ, Samson JE, Moineau S. 2010. Bacteriophage resistance mechanisms. Nat Rev Microbiol 8:317–327. https://doi.org/10.1038/nrmicro2315.

11. Sorek R, Lawrence CM, Wiedenheft B. 2013. CRISPR-mediated adaptive immune systems in bacteria and archaea. Annu Rev Biochem 82:237–266. https://doi.org/10.1146/annurev-biochem-072911-172315.

12. Roberts RJ. 2005. How restriction enzymes became the workhorses of molecular biology. Proc Natl Acad Sci U S A 102:5905–5908. https://doi.org/10.1073/pnas.0500923102.

13. Navarre WW, McClelland M, Libby SJ, Fang FC. 2007. Silencing of xenogeneic DNA by H-NS-facilitation of lateral gene transfer in bacteria by a defense system that recognizes foreign DNA. Genes Dev 21:1456–1471. https://doi.org/10.1101/gad.1543107.

14. Navarre WW, Porwollik S, Wang Y, McClelland M, Rosen H, Libby SJ, Fang FC. 2006. Selective silencing of foreign DNA with low GC content by the H-NS protein in *Salmonella*. Science 313:236–238. https://doi.org/10.1126/science.1128794.

15. Heroven AK, Nagel G, Tran HJ, Parr S, Dersch P. 2004. RovA is autoregulated and antagonizes H-NS-mediated silencing of invasin and *rovA* expression in *Yersinia pseudotuberculosis*. Mol Microbiol 53:871–888. https://doi.org/10.1111/j.1365-2958.2004.04162.x.

16. Oshima T, Ishikawa S, Kurokawa K, Aiba H, Ogasawara N. 2006. *Escherichia coli* histone-like protein H-NS preferentially binds to horizontally acquired DNA in association with RNA polymerase. DNA Res 13:141–153. https://doi.org/10.1093/dnares/dsl009.

17. Tendeng C, Soutourina OA, Danchin A, Bertin PN. 2003. MvaT proteins in *Pseudomonas spp.*: a novel class of H-NS-like proteins. Microbiology 149:3047–3050. https://doi.org/10.1099/mic.0.C0125-0.

18. Gordon B, Imperial R, Wang L, Navarre WW, Liu J. 2008. Lsr2 of *Mycobacterium* represents a novel class of H-NS-like proteins. J Bacteriol 190:7052–7059. https://doi.org/10.1128/JB.00733-08.

19. Gordon BR, Li Y, Wang L, Sintsova A, van Bakel H, Tian S, Navarre WW, Xia B, Liu J. 2010. Lsr2 is a nucleoid-associated protein that targets AT-rich sequences and virulence genes in *Mycobacterium tuberculosis*. Proc Natl Acad Sci U S A 107:5154–5159. https://doi.org/10.1073/pnas.0913551107.

20. Duan B, Ding P, Hughes TR, Navarre WW, Liu J, Xia B. 2018. How bacterial xenogeneic silencer rok distinguishes foreign from self DNA in its resident genome. Nucleic Acids Res 46:10514–10529. https://doi.org/10.1093/nar/gky836.

21. Smits WK, Grossman AD. 2010. The transcriptional regulator Rok binds A+T-rich DNA and is involved in repression of a mobile genetic element in *Bacillus subtilis*. PLoS Genet 6:e1001207. https://doi.org/10.1371/journal.pgen.1001207.

22. Gordon BR, Li Y, Cote A, Weirauch MT, Ding P, Hughes TR, Navarre WW, Xia B, Liu J. 2011. Structural basis for recognition of AT-rich DNA by unrelated xenogeneic silencing proteins. Proc Natl Acad Sci U S A 108:10690–10695. https://doi.org/10.1073/pnas.1102544108.

23. Castang S, Dove SL. 2010. High-order oligomerization is required for the function of the H-NS family member MvaT in *Pseudomonas aeruginosa*. Mol Microbiol 78:916–931. https://doi.org/10.1111/j.1365-2958.2010.07378.x.

24. Daubin V, Lerat E, Perrière G. 2003. The source of laterally transferred genes in bacterial genomes. Genome Biol 4:R57. https://doi.org/10.1186/gb-2003-4-9-r57.

25. Hildebrand F, Meyer A, Eyre-Walker A. 2010. Evidence of selection upon genomic GC content in bacteria. PLoS Genet 6:e1001107. https://doi.org/10.1371/journal.pgen.1001107.

26. Zamenhof S, Brawerman G, Chargaff E. 1952. On the desoxypentose nucleic acids from several microorganisms. Biochim Biophys Acta 9:402–405. https://doi.org/10.1016/0006-3002(52)90184-4.

27. Spurio R, Falconi M, Brandi A, Pon CL, Gualerzi CO. 1997. The oligomeric structure of nucleoid protein H-NS is necessary for recognition of intrinsically curved DNA and for DNA bending. EMBO J 16:1795–1805. https://doi.org/10.1093/emboj/16.7.1795.

28. Winardhi RS, Fu W, Castang S, Li Y, Dove SL, Yan J. 2012. Higher order oligomerization is required for H-NS family member MvaT to form gene-silencing nucleoprotein filament. Nucleic Acids Res 40:8942–8952. https://doi.org/10.1093/nar/gks669.

29. Chen JM, Ren H, Shaw JE, Wang YJ, Li M, Leung AS, Tran V, Berbenetz NM, Kocíncová D, Yip CM, Reyrat JM, Liu J. 2008. Lsr2 of *Mycobacterium tuberculosis* is a DNA-bridging protein. Nucleic Acids Res 36:2123–2135. https://doi.org/10.1093/nar/gkm1162.

30. Lim CJ, Lee SY, Kenney LJ, Yan J. 2012. Nucleoprotein filament formation is the structural basis for bacterial protein H-NS gene silencing. Sci Rep 2:509. https://doi.org/10.1038/srep00509.

31. Landick R, Wade JT, Grainger DC. 2015. H-NS and RNA polymerase: a love-hate relationship? Curr Opin Microbiol 24:53–59. https://doi.org/10.1016/j.mib.2015.01.009.

32. Will WR, Navarre WW, Fang FC. 2015. Integrated circuits: how transcriptional silencing and counter-silencing facilitate bacterial evolution. Curr Opin Microbiol 23:8–13. https://doi.org/10.1016/j.mib.2014.10.005.

33. Will WR, Bale DH, Reid PJ, Libby SJ, Fang FC. 2014. Evolutionary expansion of a regulatory network by counter-silencing. Nat Commun 5:5270. https://doi.org/10.1038/ncomms6270.

34. Caramel A, Schnetz K. 1998. Lac and lambda repressors relieve silencing of the *Escherichia coli bgl* promoter. Activation by alteration of a repressing nucleoprotein complex. J Mol Biol 284:875–883. https://doi.org/10.1006/jmbi.1998.2191.

35. Kane KA, Dorman CJ. 2011. Rational design of an artificial genetic switch: co-option of the H-NS-repressed *proU* operon by the VirB virulence master regulator. J Bacteriol 193:5950–5960. https://doi.org/10.1128/JB.05557-11.

36. Colangeli R, Helb D, Vilchèze C, Hazbón MH, Lee C-G, Safi H, Sayers B, Sardone I, Jones MB, Fleischmann RD, Peterson SN, Jacobs WR, Jr, Alland D. 2007. Transcriptional regulation of multi-drug tolerance and antibiotic-induced responses by the histone-like protein Lsr2 in *M. tuberculosis*. PLoS Pathog 3:e87. https://doi.org/10.1371/journal.ppat.0030087.

37. Colangeli R, Haq A, Arcus VL, Summers E, Magliozzo RS, McBride A, Mitra AK, Radjainia M, Khajo A, Jacobs WR, Salgame P, Alland D. 2009. The multifunctional histone-like protein Lsr2 protects mycobacteria against reactive oxygen intermediates. Proc Natl Acad Sci U S A 106:4414–4418. https://doi.org/10.1073/pnas.0810126106.

38. Pfeifer E, Hünnefeld M, Popa O, Frunzke J. 2019. Impact of xenogeneic silencing on phage-host interactions. J Mol Biol 431:4670–4683. https://doi.org/10.1016/j.jmb.2019.02.011.

39. Gehrke EJ, Zhang X, Pimentel-Elardo SM, Johnson AR, Rees CA, Jones SE, Hindra GSS, Turvey S, Boursalie S, Hill JE, Carlson EE, Nodwell JR, Elliot MA. 2019. Silencing cryptic specialized metabolism in Streptomyces by the nucleoid-associated protein Lsr2. Elife 431:e47691. https://doi.org/10.7554/eLife.47691.

40. Pfeifer-Sancar K, Mentz A, Rückert C, Kalinowski J. 2013. Comprehensive analysis of the *Corynebacterium glutamicum* transcriptome using an improved RNAseq technique. BMC Genomics 14:888. https://doi.org/10.1186/1471-2164-14-888.

41. Bailey TL, Boden M, Buske FA, Frith M, Grant CE, Clementi L, Ren J, Li WW, Noble WS. 2009. MEME Suite: tools for motif discovery and searching. Nucleic Acids Res 37:W202–W208. https://doi.org/10.1093/nar/gkp335.

42. Grant CE, Bailey TL, Noble WS. 2011. FIMO: scanning for occurrences of a given motif. Bioinformatics 27:1017–1018. https://doi.org/10.1093/bioinformatics/btr064.

43. Frunzke J, Engels V, Hasenbein S, Gätgens C, Bott M. 2008. Co-ordinated regulation of gluconate catabolism and glucose uptake in *Corynebacterium glutamicum* by two functionally equivalent transcriptional regulators, GntR1 and GntR2. Mol Microbiol 67:305–322. https://doi.org/10.1111/j.1365-2958.2007.06020.x.

44. Rojo F. 1999. Repression of transcription initiation in bacteria. J Bacteriol 181:2987–2991. https://doi.org/10.1128/JB.181.10.2987-2991.1999.

45. Rydenfelt M, Garcia HG, Cox RS, III, Phillips R. 2014. The influence of promoter architectures and regulatory motifs on gene expression in *Escherichia coli*. PLoS One 9:e114347. https://doi.org/10.1371/journal.pone.0114347.

46. Grünberger A, Probst C, Helfrich S, Nanda A, Stute B, Wiechert W, von Lieres E, Nöh K, Frunzke J, Kohlheyer D. 2015. Spatiotemporal microbial single-cell analysis using a high-throughput microfluidics cultivation platform. Cytometry A 87:1101–1115. https://doi.org/10.1002/cyto.a.22779.

47. Ding P, McFarland KA, Jin S, Tong G, Duan B, Yang A, Hughes TR, Liu J, Dove SL, Navarre WW, Xia B. 2015. A novel AT-rich DNA recognition mechanism for bacterial xenogeneic silencer MvaT. PLoS Pathog 11:e1004967. https://doi.org/10.1371/journal.ppat.1004967.

48. Lang B, Blot N, Bouffartigues E, Buckle M, Geertz M, Gualerzi CO, Mavathur R, Muskhelishvili G, Pon CL, Rimsky S, Stella S, Babu MM, Travers A. 2007. High-affinity DNA binding sites for H-NS provide a molecular basis for selective silencing within proteobacterial genomes. Nucleic Acids Res 35:6330–6337. https://doi.org/10.1093/nar/gkm712.

49. Gulvady R, Gao Y, Kenney LJ, Yan J. 2018. A single molecule analysis of H-NS uncouples DNA binding affinity from DNA specificity. Nucleic Acids Res 46:10216–10224. https://doi.org/10.1093/nar/gky826.

50. Dillon SC, Espinosa E, Hokamp K, Ussery DW, Casadesús J, Dorman CJ. 2012. LeuO is a global regulator of gene expression in *Salmonella enterica* serovar Typhimurium. Mol Microbiol 85:1072–1089. https://doi.org/10.1111/j.1365-2958.2012.08162.x.

51. Yu RR, DiRita VJ. 2002. Regulation of gene expression in *Vibrio cholerae* by ToxT involves both antirepression and RNA polymerase stimulation. Mol Microbiol 43:119–134. https://doi.org/10.1046/j.1365-2958.2002.02721.x.

52. Navarre WW, Halsey TA, Walthers D, Frye J, McClelland M, Potter JL, Kenney LJ, Gunn JS, Fang FC, Libby SJ. 2005. Co-regulation of *Salmonella enterica* genes required for virulence and resistance to antimicrobial peptides by SlyA and PhoP/PhoQ. Mol Microbiol 56:492–508. https://doi.org/10.1111/j.1365-2958.2005.04553.x.

53. Shimada T, Bridier A, Briandet R, Ishihama A. 2011. Novel roles of LeuO in transcription regulation of *E. coli* genome: antagonistic interplay with the universal silencer H-NS. Mol Microbiol 82:378–397. https://doi.org/10.1111/j.1365-2958.2011.07818.x.

54. Kurthkoti K, Tare P, Paitchowdhury R, Gowthami VN, Garcia MJ, Colangeli R, Chatterji D, Nagaraja V, Rodriguez GM. 2015. The mycobacterial iron-dependent regulator IdeR induces ferritin (*bfrB*) by alleviating Lsr2 repression. Mol Microbiol 98:864–877. https://doi.org/10.1111/mmi.13166.

55. Shin M, Song M, Rhee JH, Hong Y, Kim YJ, Seok YJ, Ha KS, Jung SH, Choy HE. 2005. DNA looping-mediated repression by histone-like protein H-NS: specific requirement of Esigma70 as a cofactor for looping. Genes Dev 19:2388–2398. https://doi.org/10.1101/gad.1316305.

56. Jordi BJ, Higgins CF. 2000. The downstream regulatory element of the *proU* operon of *Salmonella typhimurium* inhibits open complex formation by RNA polymerase at a distance. J Biol Chem 275:12123–12128. https://doi.org/10.1074/jbc.275.16.12123.

57. Nagarajavel V, Madhusudan S, Dole S, Rahmouni AR, Schnetz K. 2007. Repression by binding of H-NS within the transcription unit. J Biol Chem 282:23622–23630. https://doi.org/10.1074/jbc.M702753200.

58. Lee DJ, Minchin SD, Busby SJ. 2012. Activating transcription in bacteria. Annu Rev Microbiol 66:125–152. https://doi.org/10.1146/annurev-micro-092611-150012.

59. Zwir I, Latifi T, Perez JC, Huang H, Groisman EA. 2012. The promoter architectural landscape of the *Salmonella* PhoP regulon. Mol Microbiol 84:463–485. https://doi.org/10.1111/j.1365-2958.2012.08036.x.

60. Sanchez A, Osborne ML, Friedman LJ, Kondev J, Gelles J. 2011. Mechanism of transcriptional repression at a bacterial promoter by analysis of single molecules. EMBO J 30:3940–3946. https://doi.org/10.1038/emboj.2011.273.

61. Kinoshita S, Udaka S, Shimono M. 1957. Studies on the amino acid fermentation. Part 1. Production of L-glutamic acid by various microorganisms. J Gen Appl Microbiol 3:193–205. https://doi.org/10.2323/jgam.3.193.

62. Kensy F, Zang E, Faulhammer C, Tan RK, Büchs J. 2009. Validation of a high-throughput fermentation system based on online monitoring of biomass and fluorescence in continuously shaken microtiter plates. Microb Cell Fact 8:31. https://doi.org/10.1186/1475-2859-8-31.

63. Grünberger A, Paczia N, Probst C, Schendzielorz G, Eggeling L, Noack S, Wiechert W, Kohlheyer D. 2012. A disposable picolitre bioreactor for cultivation and investigation of industrially relevant bacteria on the single cell level. Lab Chip 12:2060–2068. https://doi.org/10.1039/c2lc40156h.

64. Sambrook J, Russel DW. 2001. Molecular cloning: a laboratory manual, 3rd ed. Cold Spring Harbor Laboratory Press, Cold Spring Harbor, NY.

65. Gibson DG, Young L, Chuang RY, Venter JC, Hutchison CA, III, Smith HO. 2009. Enzymatic assembly of DNA molecules up to several hundred kilobases. Nat Methods 6:343–345. https://doi.org/10.1038/nmeth.1318.

66. Eikmanns BJ, Thum-Schmitz N, Eggeling L, Ludtke KU, Sahm H. 1994. Nucleotide sequence, expression and transcriptional analysis of the *Corynebacterium glutamicum gltA* gene encoding citrate synthase. Microbiology 140:1817–1828. https://doi.org/10.1099/13500872-140-8-1817.

67. Niebisch A, Bott M. 2001. Molecular analysis of the cytochrome bc_1-aa_3 branch of the *Corynebacterium glutamicum* respiratory chain containing an unusual diheme cytochrome c_1. Arch Microbiol 175:282–294. https://doi.org/10.1007/s002030100262.

68. Ettwiller L, Buswell J, Yigit E, Schildkraut I. 2016. A novel enrichment strategy reveals unprecedented number of novel transcription start sites at single base resolution in a model prokaryote and the gut microbiome. BMC Genomics 17:199. https://doi.org/10.1186/s12864-016-2539-z.

69. Kalinowski J, Bathe B, Bartels D, Bischoff N, Bott M, Burkovski A, Dusch N, Eggeling L, Eikmanns BJ, Gaigalat L, Goesmann A, Hartmann M, Huthmacher K, Krämer R, Linke B, McHardy AC, Meyer F, Möckel B, Pfefferle W, Pühler A, Rey DA, Rückert C, Rupp O, Sahm H, Wendisch VF, Wiegräbe I, Tauch A. 2003. The complete *Corynebacterium glutamicum* ATCC 13032 genome sequence and its impact on the production of L-aspartate-derived amino acids and vitamins. J Biotechnol 104:5–25. https://doi.org/10.1016/s0168-1656(03)00154-8.

70. R Development Core Team. 2016. R: a language and environment for statistical computing. R Foundation for Statistical Computing, Vienna, Austria.